




## Article

# Effect of Angle, Temperature and Vacancy Defects on Mechanical Properties of PSI-Graphene

Lu Xie <sup>1,\*</sup>, Tingwei Sun <sup>1</sup>, Chenwei He <sup>2</sup>, Haojie An <sup>1</sup>, Qin Qin <sup>1</sup> and Qing Peng <sup>3,\*</sup>

<sup>1</sup> School of Mechanical Engineering, University of Science and Technology Beijing, Beijing 100083, China; suntiwei@xs.ustb.edu.cn (T.S.); anhaojie@xs.ustb.edu.cn (H.A.); qinqin@me.ustb.edu.cn (Q.Q.)

<sup>2</sup> China Nuclear Power Technology Research Institute Co., Ltd., Reactor Engineering and Safety Research Center, Shenzhen 518031, China; hechenwei@cgnpc.com.cn

<sup>3</sup> Nuclear Engineering and Radiological Sciences, University of Michigan, Ann Arbor, MI 48108, USA

\* Correspondence: xielu@ustb.edu.cn (L.X.); q@qpeng.org (Q.P.)

Received: 30 March 2019; Accepted: 4 May 2019; Published: 6 May 2019



**Abstract:** The PSI-graphene, a two-dimensional structure, was a novel carbon allotrope. In this paper, based on molecular dynamics simulation, the effects of stretching direction, temperature and vacancy defects on the mechanical properties of PSI-graphene were studied. We found that when PSI-graphene was stretched along 0° and 90° at 300 K, the ultimate strength reached a maximum of about 65 GPa. And when stretched along 54.2° and 155.2° at 300 K, the Young's modulus had peaks, which were 1105 GPa and 2082 GPa, respectively. In addition, when the temperature was raised from 300 K to 900 K, the ultimate strength in all directions was reduced. The fracture morphology of PSI-graphene stretched at different angles was also shown in the text. In addition, the number of points removed from PSI-graphene sheet also seriously affected the tensile properties of the material. It was found that, compared with graphene, PSI-graphene didn't have the negative Poisson's ratio phenomenon when it was stretched along the direction of 0°, 11.2°, 24.8° and 34.7°. Our results provided a reference for studying the multi-angle stretching of other carbon structures at various temperatures.

**Keywords:** PSI-graphene; mechanical properties; stretching direction; fracture morphology; vacancy defects

## 1. Introduction

Carbon possesses a variety of hybridization methods, such as  $sp$ ,  $sp^2$  and  $sp^3$ , so that a variety of carbon allotropes are formed, which include graphene, carbon honeycomb (CHC), carbon nanotube and graphite and so on. These carbon allotropes have unique properties due to their different structures [1]. Graphene, a two-dimensional carbon structure, exhibits outstanding physical, chemical, mechanical properties, thermodynamic and other properties under large strains [2–5]. CHC [6–8] is a new 3D carbon allotrope in a honeycomb lattice and has wide application prospects. Similar to graphene, PSI-graphene was a novel two-dimensional allotrope of carbon, which is formed by a 5-6-7 carbon ring. Based on first-principles calculations, it is dynamically and thermally stable [1].

A large number of studies have been carried out to explore the mechanical properties of carbon allotropes [9–11]. The mechanical properties of the material were judged by parameters such as ultimate strength, fracture strain, Poisson's ratio, and the Young's modulus of the structure. Poisson's ratio is a mechanical parameter describing the transverse strain of materials in response to the axial deformation. Most solid materials shrink transversely when they are stretched in the longitudinal direction, resulting in a positive Poisson's ratio (PPR) value. However, the abnormal ones, known as auxetics, will exhibit transverse expansion [12]. The ultimate strength is the maximum stress of the material at breaking point and the fracture strain is the strain at the time of failure of the material.

Young's modulus is the ratio of stress to strain in the linear range. Zhao et al. [13] investigated the mechanical properties of super graphene, cyclographene and graphene, and given the relationship between the Young's modulus, shear modulus, Poisson's ratio, ultimate strength and ultimate strain along the armchair and zigzag direction. Based on first-principles calculation and molecular dynamics (MD) simulation, Jiang et al. [14] proposed twin graphene, a two-graphene (2D) semiconducting carbon allotropes, and also studied the mechanical properties, including in-plane stiffness, Poisson's ratio, shear stiffness and bending stiffness. Jing et al. [15] studied the effect of vacancy and Stone–Wales (SW) defects on the Young's modulus of graphene by MD simulation. It was found that the Young's modulus decreased as the degree of defects increased. Through MD simulation, Deng et al. [10] found that graphene had a negative Poisson's ratio when uniaxially stretched, and this phenomenon still existed at a temperature of 2400 K. Based on MD simulations, Dewapriya et al. [16] studied the effects of nanoscale vacancies on cracks under uniaxial tensile tests and found that the nanoscale central crack can be arrested by the strategic positioning of symmetric nanoscale holes. By combining the continuous elastic theory with the tight-binding atomic simulation, Cadelano et al. [17] obtained the nonlinear stress-strain curve of the graphene and the corresponding elastic modulus during stretching. Treacy et al. [18] estimated the Young's modulus of carbon nanotubes by transmission electron microscopy. It had also been found that the Young's modulus of CNT was particularly large, in the terapascal (TPa) range. Therefore, it can be used as a nanoscale fiber in lightweight composite materials. Besides, our team had also conducted a great deal of research on carbon honeycomb.

Lots of research has also been carried out to study the thermodynamic and other properties of carbon allotropes. Chen et al. [19] studied the thermal transport properties of carbon honeycomb with different chirality by equilibrium molecular dynamics (EMD) simulation and found that the thermal conductivity along the honeycomb axis was three times that of the other axes. The results also contributed to guiding the development of carbon honeycomb thermal channeling devices. Wei et al. [20] also studied the thermal conductivities of the newly synthesized all- $sp^2$  three-dimensional graphene. Gao et al. [21] studied the thermal conductivities characteristics of two-layer graphene with different layer cutting patterns and assembly structures during stretching and proved the potential application of graphene in the field of thermal conduction. Both Evans et al. [22] and Hu et al. [23] studied the thermal conduction of graphene by MD. It was found that the smooth edge has a higher thermal conductivity than the rough edge, the direction of zigzag and armchair had similar thermal conductivity. Moreover, Liu et al. [24] studied the electrical properties of T-graphene, a two-dimensional carbon allotrope with tetrarings by first-principles calculations. It was proved that T-graphene also had Dirac-like fermions and a high Fermi velocity. AH et al. [25] studied the electronic properties of graphene stacks and also introduced the effects of electron-electron and electron-phonon interactions in single-layer and multi-layer graphene. Kuilla et al. [26] utilized graphene to prepare nanocomposites with different polymer matrixes. Based on density functional theory, Gu et al. [27] found that the formation of  $sp^3$  carbon-carbon bonds would make the structure more stable and further study the mechanical and thermodynamic properties of carbon honeycomb with different chiralities.

Compared with graphene, carbon honeycomb and other carbon structure, scholars had less research on PSI-graphene. Li et al. proposed a two-dimensional PSI-graphene structure constructed by polymerizing the carbon skeletons of sindacenes based on first-principles calculations and found that the structure also can be used as an anode material for lithium-ion batteries [1]. Currently, there is no evidence that PSI-graphene can be made experimentally. If conditions permit, our team will continue to follow up on PSI-graphene research. In addition, the PSI graphene sheets and the stone wales structure is different. PSI-graphene consists of regular polygons, and the stone-wales structure consists of polygons. The polygon arrangement of PSI-graphene is very different from the stone-wales structure.

In this paper, PSI-graphene has been studied in multi-angle stretching. At the same time, the ultimate strength, the Young's modulus and failure morphology of PSI-graphene were observed when stretching at different angles. Compared with graphene, the Poisson's ratio of the two structures was

analyzed. Besides, the effect of temperature and vacancy defects on mechanical properties has also been explored.

## 2. Materials and Methods

The model of PSI-graphene and graphene is shown in Figure 1. The PSI-graphene structure was constructed from pentagonal, hexagonal and heptagon carbon rings [28], which was dynamically and thermally stable, calculated by state-of-the-art first-principles. Figure 1 illustrated that the PSI-graphene and graphene sheets were stretched along different directions in the x-y plane.  $\theta$  was the shifting angle away from the symmetry axis and  $\alpha$  was the shifting angle away from the armchair direction. Graphene was a six-fold rotational symmetry structure. The angle of the armchair and zigzag direction is  $30^\circ$ . The shifting angles of graphene between  $0^\circ$  and  $30^\circ$  were selected. Other shifting angles were obtained by the symmetry of a graphene sheet. The PSI-graphene sheet was axisymmetric structure, and the shifting angle was selected between  $0^\circ$  and  $180^\circ$ .

MD method was widely used in many fields [29,30]. All studies in this paper were performed by MD simulations based on the Large-scale Atomic/Molecular Massively Parallel Simulator (LAMMPS) package [31]. In order to describe the interatomic force between carbon atoms, we used the adaptive intermolecular reactive empirical bond order (AIREBO) potential function, which was widely used in the interaction between carbon structure atoms, such as graphene [32], carbon nanotube [33] and CHC [34].

The shifting angle  $\theta$  and  $\alpha$ , shown in Figure 1, defined the stretching direction in the simulation. The shifting angle should be carefully selected so that the structure meets the periodic boundary conditions in both x and y directions to reduce the edge effect. Eight PSI-graphene samples were carefully selected with  $\theta$  of  $0^\circ$ ,  $11.2^\circ$ ,  $24.8^\circ$ ,  $34.7^\circ$ ,  $54.2^\circ$ ,  $90^\circ$ ,  $125.8^\circ$  and  $155.2^\circ$ . In addition, to avoid size effects, all the simulations were performed on PSI-graphene sheets with similar size. According to the study of graphene multi-angle stretching [12], we constructed the model of PSI-graphene sheets with about 18,000 atoms. In all simulations, periodic boundary conditions along the x and y directions and fixed boundary conditions along the z direction were used. It is fixed in the z direction, so PSI-graphene sheets don't fluctuate. The time step was 0.5 fs. An NPT ensemble was employed at the specific temperature (300 K, 500 K, 700 K and 900 K respectively) and zero pressure. The NPT ensemble was performed for all the simulations, including the relaxing stage and tensile stage. The external pressure was zero at the relaxing stage. However, at the tensile stage, external pressure in tensile direction was not controlled, since the stress was calculated by the pressure in the tensile direction. In addition, the simulated time is strain rate timing tensile strain. The trajectories of the relaxing stage were recorded every 5000 time steps, while the trajectories of the tensile stage were recorded every 8000 time steps. In addition, the data of the stress-strain curve were output every 500 time steps. Under the NPT ensemble, the relax stage is 25ps and the tensile stage is 150ps. To avoid the thermal and pressure effect, the temperature and pressure of simulation were controlled by the Nose-Hoover thermostat and barostat. The PSI-graphene samples were stretched in the x direction with an engineering strain rate of  $10^9 \text{ s}^{-1}$ . The post-processing and results visualization were performed by OVITO [35].

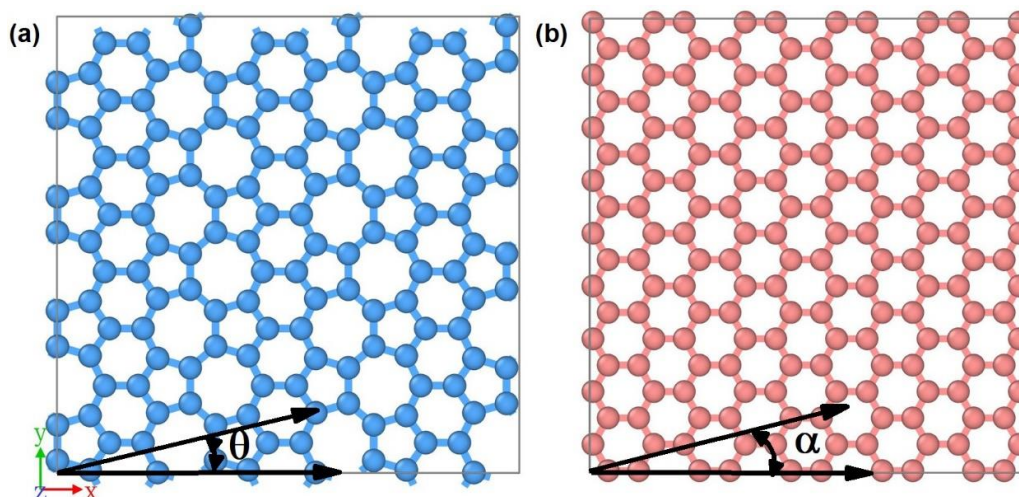


**Figure 1.** Schematic diagram of (a) PSI-graphene and (b) graphene for loading along different directions in the x-y plane.  $\theta$  and  $\alpha$  are the shifting angles of the stretching direction.

### 3. Results and Discussions

#### 3.1. Mechanical Properties of Structure at Stretching along Different Angles

To investigate the effect of shifting angle on the mechanical properties of PSI-graphene sheets, series of MD simulations of PSI-graphene sheets with different shifting angles were carried out at the temperature of 300 K. The strains in the x and y directions were represented by  $\epsilon_x$  and  $\epsilon_y$ , respectively. The tensile results were cautiously reported in the part where  $\epsilon_x$  was up to 0.1 [10]. Figure 2 showed the curves of strain  $\epsilon_x$  vs  $\epsilon_y$  for PSI-graphene and graphene sheets at 300 K. The curves of PSI-graphene (Figure 2a) were monotonically decreasing for angles of  $0^\circ$ ,  $11.2^\circ$ ,  $24.8^\circ$  and  $34.7^\circ$  in Figure 2a. The curves of graphene (as shown in Figure 2b) showed a different trend. It can be found that the curve decreased and then increased when the graphene was stretched at shifting angle of  $0^\circ$  and  $10.9^\circ$  and the curves were monotonically decreased at shifting angle of  $25.3^\circ$  and  $30^\circ$ . Compared with graphene, it can be seen that the PSI-graphene structure didn't have a negative

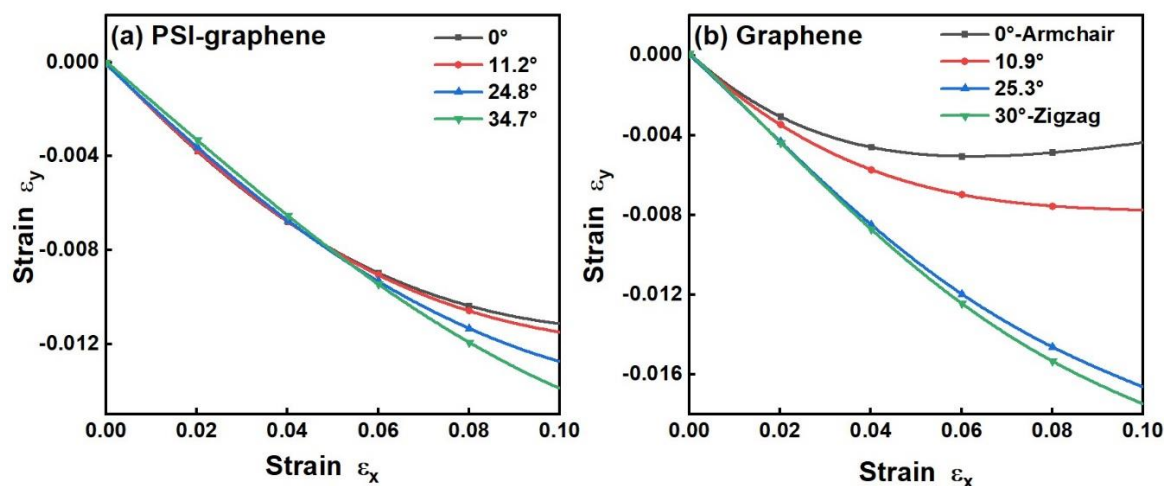


**Figure 2.** The curves of strain  $\epsilon_x$  vs  $\epsilon_y$  for two structures on the stretching direction at 300 K. (a) PSI-graphene (b) graphene.

The mechanical properties of PSI-graphene and graphene can be described by two independent constants, i.e., ultimate strength and Young's modulus. According to the characteristics of PSI-graphene and graphene sheets, the range between  $0^\circ$  and  $180^\circ$  was observed in Figure 3a,b, and the range



between 0° and 30° was observed in Figure 3c,d. The formula for calculating Young's modulus is as follows.

$$E = \frac{\sigma}{A}. \quad (1)$$

E—Young's modulus;  $\sigma$ —stress; A—strain.

The ultimate strength of the PSI-graphene sheet at different angles as shown in Figure 3a at 300 K. There are four peaks at 0°, 90°, 180° and 270°, about 64 GPa at 0° and 180°, 65 GPa at 90° and 270°. It can be considered that the material had the same mechanical properties and tensile strength when stretched at angles of 0°, 90°, 180° and 270°. The ultimate strength had a minimum at the 54.2° about 55 GPa. And the ultimate strength was reduced by about 15%. The Young's modulus of the PSI-graphene sheet was shown in the Figure 3b at 300 K. It was clear that there were four peaks at 54.2°, 155.2°, 234.2°, and 335.2°, about 1105 GPa at 54.2° and about 2082 GPa at 155.2°. The maximum value of the Young's modulus at 155.2° was about twice that of at 54.2°. At other angles, the Young's modulus value fluctuated little and was distributed around 800 GPa.

Figure 3c presents the ultimate strength of the graphene sheet at different angles at 300 K. Compared with PSI-graphene, the curves had six peaks at 30°, 90°, 150°, 210°, 270° and 330° and the ultimate strength was 105 GPa. At 0°, 60°, 120°, 180°, 240° and 300°, the ultimate strength value was the smallest, about 86 GPa. The strength was reduced by about 17.5%. In Figure 3d, the Young's modulus distribution was completely different, with peaks at 30°, 90°, 150°, 210°, 270° and 330°. The Young's modulus was 1033 GPa at 0°. The Young's modulus had a minimum in the direction of 0°, 60°, 120°, 180°, 240° and 300°, which was 903 GPa [36]. The Young's modulus was reduced by about 12.6%.

In a word, the tensile strength of PSI-graphene sheets was the best when stretched along the 0° and 90° directions, which was slightly larger than that stretched along other angles. But the strength of PSI-graphene was slightly lower than that of graphene.

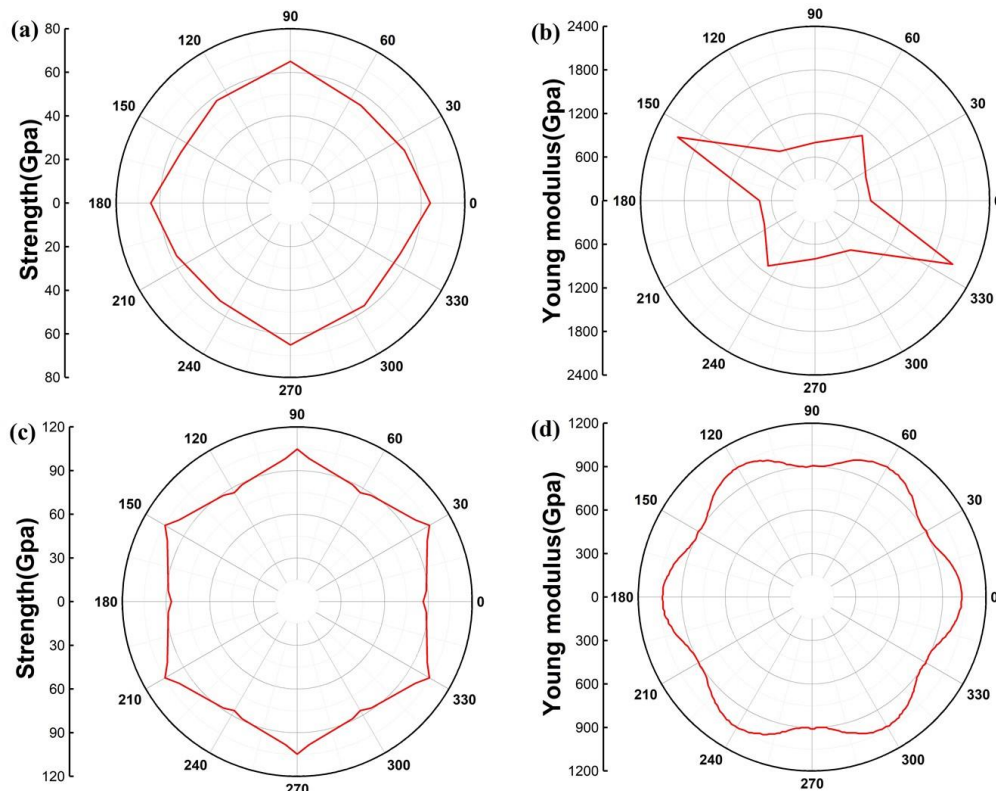


**Figure 3.** The polar coordinate curve of (a) ultimate strength and (b) the Young's modulus of PSI-graphene and (c) ultimate strength and (d) the Young's modulus [36] of graphene with different stretching directions at 300K.

### 3.2. Fracture Morphology of PSI-Graphene and Graphene

In this section, compared with graphene, the fractured state of PSI-graphene was studied. Here, the von Mises strains (scales from 0 to 1) has been employed to study the local atomic strains by using OVITO with a cutoff radius of 3.5 Å. The von Mises strain is based on the distortion energy of a structure and is widely used in biomechanical studies [37]. Figure 4 exhibited the evolution of local shear strains for loading along stretching direction. Figure 4a illustrated the failure morphology of PSI-graphene at different shifting angles when the crack surface was generated. With  $\theta = 0^\circ$ ,  $24.8^\circ$ ,  $54.2^\circ$  and  $90^\circ$ , crack surfaces in the x-y plane was a straight line, which was substantially perpendicular to the direction of stretching.

The failure morphology of graphene at different shifting angles is shown in Figure 4b. For graphene, the angle between the direction of the armchair was selected as the  $\alpha$ . It was found that the cracked surface of graphene in the zigzag direction shows two crossed branches. The angle between the two branches was about  $120^\circ$  (or  $60^\circ$ ) [36]. And, the same result was obtained when  $\theta = 25.3^\circ$ . However, in the direction of armchair ( $0^\circ$ ) and  $55.3^\circ$ , the crack was a straight line along the zigzag direction.

The crack morphology in the x-y plane was completely different for PSI-graphene and graphene at  $24.8^\circ$  and  $90^\circ$ . The PSI-graphene sheet mainly produced cracks at the direction that was perpendicular to the direction of stretching. For graphene, cracks inclined to extend along the zigzag direction in the plane. In general, it can be inferred that fractures of PSI-graphene and graphene were similar at  $0^\circ$  and  $54.2^\circ$ , while at angles of  $24.8^\circ$  and  $90^\circ$ , the fractures are different. It can be seen from the figure that the shear strain was the largest at the crack.

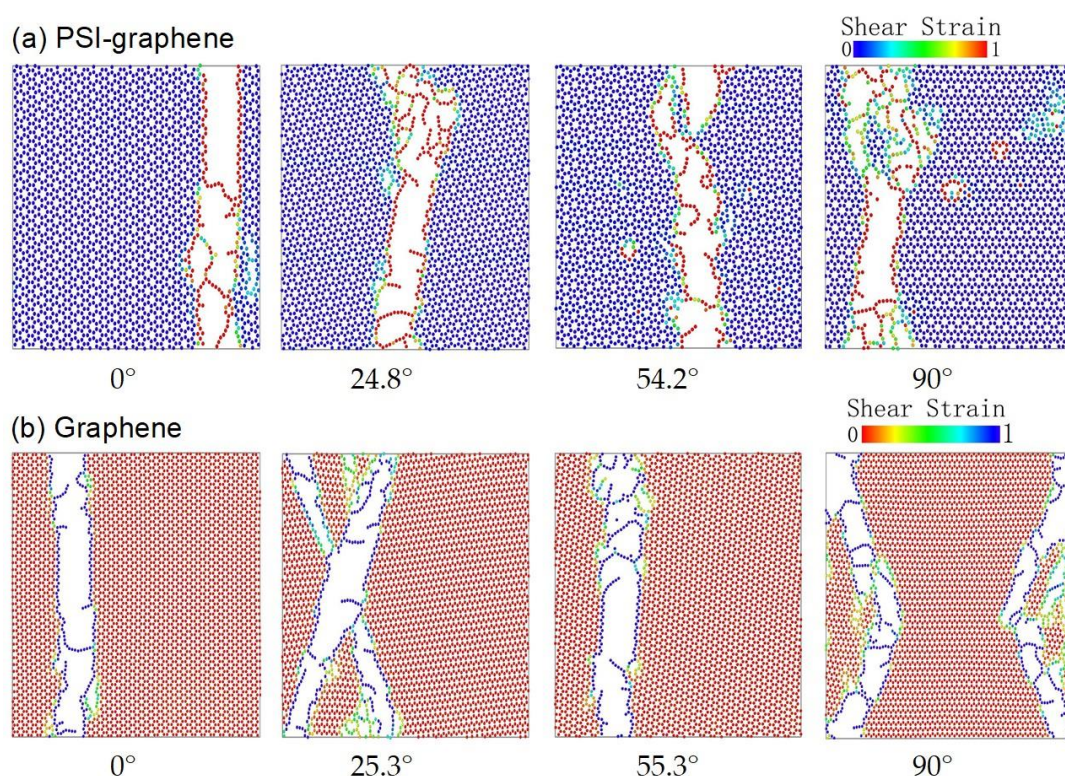


**Figure 4.** Failure morphology of (a) PSI-graphene and (b) graphene at different shifting angles at 300 K.

### 3.3. Effect of Temperature on Fracture Behavior of PSI-Graphene

To get more information about the coupled effects of temperature and angle on the fracture strength, additional simulations were performed on PSI-graphene and graphene at different temperature and angles. The results were plotted in Figure 5, in which the position of the curves represented sensitivity to temperature.

It can be observed from Figure 5a that when the temperature was changed from 300 K to 900 K, the ultimate strength gradually reduced. At 300K, the ultimate strength value was in the range of 55 to 65 GPa, while at 900 K the ultimate strength value was in the range of 32 to 43 GPa. The strength decreased by ~40% at various angles. It can be found from Figure 5a that the ultimate strength in the 0° and 90° directions was greater than the other directions at the same temperature. This result was in perfect harmony with the above studies. Figure 5b showed the curves of ultimate strength of graphene sheets at different temperatures and angles. The ultimate strength gradually increased and reached a maximum at 30°. From 300 K to 900 K, the ultimate strength of the armchair (0°) direction was 86 GPa, 78 GPa, 69 GPa and 62 GPa, while the zigzag directions (30°) were 105 GPa, 93 GPa, 85 GPa and 76 GPa, respectively. Besides, at the direction of armchair (0°) and zigzag (30°), the ultimate strength increased by 38.7% and 38.8% respectively. As the temperature increased, the ultimate strength of the material decreased and the mechanical properties of the PSI-graphene deteriorate.

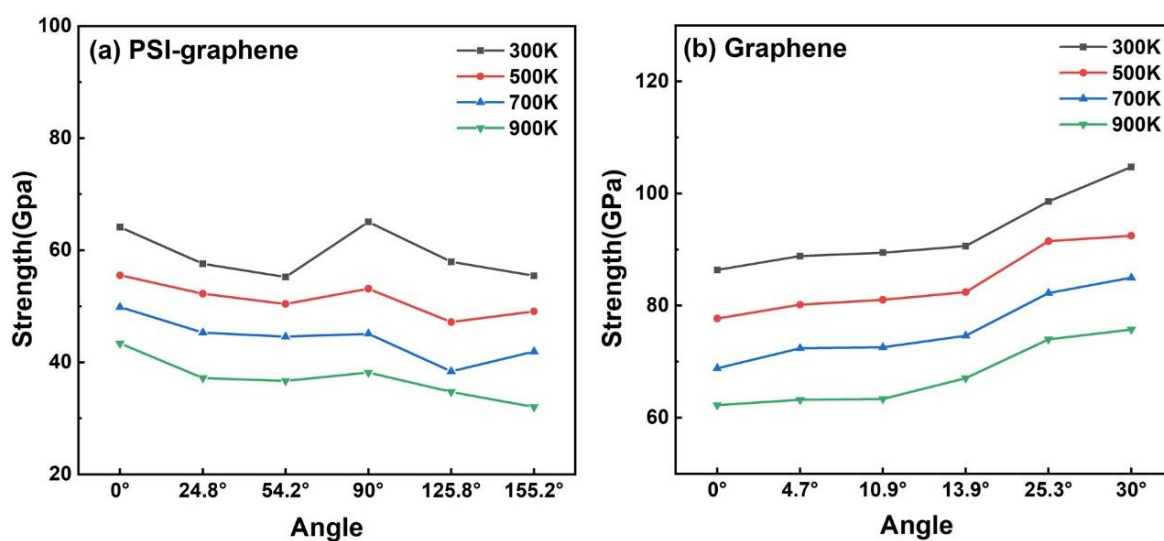


Figure 5. The strength curves of (a) PSI-graphene and (b) graphene at different temperatures and angles.

### 3.4. Effect of Vacancy Defects on Fracture Behavior of PSI-Graphene

This section elucidated the effect of point defects on the fracture behavior of PSI-graphene and graphene. The absence of atoms from the lattice of PSI-graphene and graphene was usually termed as vacancy defects, which are divided into mono-vacancy and multi-vacancy defects based on the number of atoms absent from the lattice of PSI-graphene [38]. In order to study the effect of vacancy defects on the fracture behavior of PSI-graphene and graphene, additional simulations were performed, with 0, 1, 50, 100 and 200 atoms removed from the PSI-graphene and graphene structure.

The stress-strain curve of PSI-graphene with vacancy defects is shown in Figure 6a. It can be inferred from the graph that the ultimate strength of PSI-graphene decreased with the increase of the number of absent atoms inside the structure. When the PSI-graphene sheet had no points missing, the ultimate strength of the structure was 64 GPa. When the PSI-graphene sheet was missing 1, 50, 100 and 200 atoms, the ultimate strengths were 54 GPa, 50 GPa, 44 GPa, 42 GPa, the ultimate strength was reduced by about 16%, 22%, 31% and 35%, respectively. Figure 6b shows the stress-strain curves of graphene with different point defects. It can be found that when the graphene sheet had no point defects, the ultimate strength was 86 GPa. When the graphene sheet was removed 1, 50, 100 and 200 atoms, the ultimate strengths were 75 GPa, 70 GPa, 66 GPa and 59 GPa, and the rates of decline were 13%, 19%, 23% and 31%, respectively. In summary, the presence of vacancy defects could impair the tensile strength of the PSI-graphene and graphene sheets.



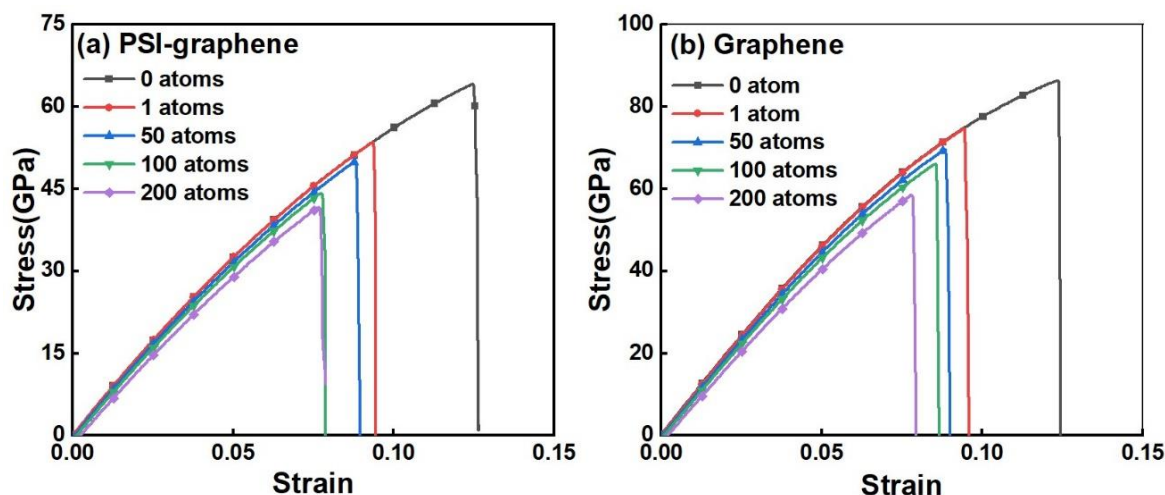


Figure 6. The Stress-Strain curves of (a) PSI-graphene and (b) graphene with different vacancy defects.

#### 4. Conclusions

In this work, MD simulations were carried out to study the effects of shifting angle, temperature and vacancy defects on the mechanical properties of the PSI-graphene. With the help of stress and strain data, it was proposed that the identical ultimate strengths and the Young's modulus of PSI-graphene were observed at 300 K. When PSI-graphene was stretched along  $0^\circ$  and  $90^\circ$  at 300 K, the ultimate strength reached a maximum of about 65 GPa. When PSI-graphene was stretched along  $54.2^\circ$  and  $155.2^\circ$  at 300 K, the Young's modulus reached the maximum, which were 1105 GPa and 2082 GPa, respectively. Moreover, the fracture morphologies of PSI-graphene in every angle were also observed at 300 K. It was found from the fracture morphologies that the crack was always perpendicular to the stretching direction of the PSI-graphene sheet and the crack extended in a straight line. As the temperature increased, the ultimate strength gradually decreased. At 300 K, the ultimate strength value was in the range of 55 to 65 GPa, while at 900 K the ultimate strength value was in the range of 32 to 43 GPa. The strength was approximately decreased by 40% at every angle when the temperature was increased from 300 K to 900 K. In addition, the number of the atom removed from PSI-graphene also seriously affected the tensile properties of the material. When the PSI-graphene sheet had no atoms missing, the ultimate strength of the structure was 65 GPa. When the PSI-graphene sheet was missing 1, 50, 100 and 200 atoms, the ultimate strength was 54 GPa, 50 GPa, 44 GPa, 42 GPa, the ultimate strength was reduced by about 16%, 22%, 31% and 35%, respectively. In addition, compared with graphene, it was known that PSI-graphene didn't have a negative Poisson's ratio phenomenon.

By comparing PSI-graphene with graphene, we found that PSI-graphene is less sensitive to temperature. When the temperature is varied from 300K to 900K, the change of PSI-graphene intensity is about 30 GPa, and the change of graphene intensity is about 50 GPa. Li et al. [1] found that PSI-graphene can be used as a battery anode material. Based on this temperature-insensitive PSI-graphene, we can use PSI-graphene instead of graphene as the battery electrode material. However, by comparing PSI-graphene with graphene, we also found that the tensile properties of graphene are better than PSI-graphene at the same temperature. Moreover, PSI-graphene does not have auxetic, which makes PSI-graphene not have the following applications, such as protective structures (e.g., body armor and shock absorber), novel biomedical structures (e.g., artificial blood vessels, ligament anchors), and traditional mechanical components (e.g., aero-engine blades and wing panels). In the case of vacancy defects, the mechanical properties of graphene are also worse than those of PSI-graphene.

These results may help in the design of PSI-graphene-based on a larger scale, which could exploit such properties of this material. It also may contribute to the study of the mechanical properties of other carbon allotropes.



**Author Contributions:** Conceptualization, L.X. and Q.P.; methodology, L.X.; software, T.S.; validation, Q.Q. and C.H.; formal analysis, H.A.; investigation, T.S.; data curation, T.S.; writing—original draft preparation, T.S.; writing—review and editing, L.X. and Q.P.; visualization, T.S. and H.A.; supervision, L.X.; project administration, L.X.; funding acquisition, L.X.

**Funding:** This research was funded by the National Natural Science Foundation of China (21703007) and the Fundamental Research Funds for the Central Universities (FRF-GF-18-011B).

**Conflicts of Interest:** The authors declare no conflict of interest.

## References

- Li, X.; Wang, Q.; Jena, P. psi-Graphene: A New Metallic Allotrope of Planar Carbon with Potential Applications as Anode Materials for Lithium-Ion Batteries. *J. Phys. Chem. Lett.* **2017**, *8*, 3234–3241. [[CrossRef](#)]
- Blees, M.K.; Barnard, A.W.; Rose, P.A.; Roberts, S.P.; McGill, K.L.; Huang, P.Y.; Ruyack, A.R.; Kevek, J.W.; Kobrin, B.; Muller, D.A.; et al. Graphene kirigami. *Nature* **2015**, *524*, 204–207. [[CrossRef](#)] [[PubMed](#)]
- Ghosh, S.; Calizo, I.; Teweldebrhan, D.; Pokatilov, E.P.; Nika, D.L.; Balandin, A.A.; Bao, W.; Miao, F.; Lau, C.N. Extremely high thermal conductivity of graphene: Prospects for thermal management applications in nanoelectronic circuits. *Appl. Phys. Lett.* **2008**, *92*. [[CrossRef](#)]
- Geim, A.K. Graphene: Status and prospects. *Science* **2009**, *324*, 1530–1534. [[CrossRef](#)]
- Bonaccorso, F.; Colombo, L.; Yu, G.; Stoller, M.; Tozzini, V.; Ferrari, A.C.; Ruoff, R.S.; Pellegrini, V. 2D materials. Graphene, related two-dimensional crystals, and hybrid systems for energy conversion and storage. *Science* **2015**, *347*, 1246501. [[CrossRef](#)] [[PubMed](#)]
- Krainyukova, N.V.; Zubarev, E.N. Carbon Honeycomb High Capacity Storage for Gaseous and Liquid Species. *Phys. Rev. Lett.* **2016**, *116*, 055501. [[CrossRef](#)]
- Wang, S.; Wu, D.; Yang, B.; Ruckenstein, E.; Chen, H. Semimetallic carbon honeycombs: New three-dimensional graphene allotropes with Dirac cones. *Nanoscale* **2018**, *10*, 2748–2754. [[CrossRef](#)]
- Qin, Q.; An, H.; He, C.; Xie, L.; Peng, Q.J.N. Anisotropic and temperature dependent mechanical properties of carbon honeycomb. *Nanotechnology* **2019**. [[CrossRef](#)] [[PubMed](#)]
- Cao, Q.; Geng, X.; Wang, H.; Wang, P.; Liu, A.; Lan, Y.; Peng, Q. A Review of Current Development of Graphene Mechanics. *Crystals* **2018**, *8*, 357. [[CrossRef](#)]
- Deng, B.; Hou, J.; Zhu, H.; Liu, S.; Liu, E.; Shi, Y.; Peng, Q. The normal-auxeticity mechanical phase transition in graphene. *2D Mater.* **2017**, *4*, 021020. [[CrossRef](#)]
- Peng, Q.; Han, L.; Lian, J.; Wen, X.; Liu, S.; Chen, Z.; Koratkar, N.; De, S. Mechanical degradation of graphene by epoxidation: Insights from first-principles calculations. *Phys. Chem. Chem. Phys.* **2015**, *17*, 19484–19490. [[CrossRef](#)]
- Hou, J.; Deng, B.; Zhu, H.; Lan, Y.; Shi, Y.; De, S.; Liu, L.; Chakraborty, P.; Gao, F.; Peng, Q. Magic Auxeticity Angle of Graphene. *Carbon* **2019**, *149*, 350–354. [[CrossRef](#)]
- Zhao, J.; Wei, N.; Fan, Z.; Jiang, J.W.; Rabczuk, T. The mechanical properties of three types of carbon allotropes. *Nanotechnology* **2013**, *24*, 095702. [[CrossRef](#)]
- Jiang, J.-W.; Leng, J.; Li, J.; Guo, Z.; Chang, T.; Guo, X.; Zhang, T. Twin graphene: A novel two-dimensional semiconducting carbon allotrope. *Carbon* **2017**, *118*, 370–375. [[CrossRef](#)]
- Jing, N.; Xue, Q.; Ling, C.; Shan, M.; Zhang, T.; Zhou, X.; Jiao, Z. Effect of defects on Young's modulus of graphene sheets: A molecular dynamics simulation. *RSC Adv.* **2012**, *2*, 9124–9129. [[CrossRef](#)]
- Dewapriya, M.A.N.; Meguid, S.A. Atomistic simulations of nanoscale crack-vacancy interaction in graphene. *Carbon* **2017**, *125*, 113–131. [[CrossRef](#)]
- Cadelano, E.; Palla, P.L.; Giordano, S.; Colombo, L. Nonlinear elasticity of monolayer graphene. *Phys. Rev. Lett.* **2009**, *102*, 235502. [[CrossRef](#)] [[PubMed](#)]
- Treacy, M.M.J.; Ebbesen, T.W.; Gibson, J.M. Exceptionally high Young's modulus observed for individual carbon nanotubes. *Nature* **1996**, *381*, 678. [[CrossRef](#)]
- Chen, X.K.; Liu, J.; Du, D.; Xie, Z.X.; Chen, K.Q. Anisotropic thermal conductivity in carbon honeycomb. *J. Phys. Condens. Matter* **2018**, *30*, 155702. [[CrossRef](#)]
- Wei, Z.; Yang, F.; Bi, K.; Yang, J.; Chen, Y. Thermal transport properties of all- sp<sup>2</sup> three-dimensional graphene: Anisotropy, size and pressure effects. *Carbon* **2017**, *113*, 212–218. [[CrossRef](#)]

21. Gao, Y.; Xu, B. van der Waals Graphene Kirigami Heterostructure for Strain-Controlled Thermal Transparency. *ACS Nano* **2018**, *12*, 11254–11262. [[CrossRef](#)] [[PubMed](#)]
22. Evans, K.E.; Alderson, A. Auxetic Materials: Functional Materials and Structures from Lateral Thinking! *Adv. Mater.* **2000**, *12*, 617–628. [[CrossRef](#)]
23. Hu, J.; Ruan, X.; Chen, Y.P.J.N. Thermal conductivity and thermal rectification in graphene nanoribbons: A molecular dynamics study. *Nano Lett.* **2009**, *9*, 2730–2735. [[CrossRef](#)]
24. Liu, Y.; Wang, G.; Huang, Q.; Guo, L.; Chen, X. Structural and electronic properties of T graphene: A two-dimensional carbon allotrope with tetrarings. *Phys. Rev. Lett.* **2012**, *108*, 225505. [[CrossRef](#)]
25. Castro Neto, A.H.; Guinea, F.; Peres, N.M.R.; Novoselov, K.S.; Geim, A.K. The electronic properties of graphene. *Rev. Mod. Phys.* **2009**, *81*, 109–162. [[CrossRef](#)]
26. Kuilla, T.; Bhadra, S.; Yao, D.; Kim, N.H.; Bose, S.; Lee, J.H. Recent advances in graphene based polymer composites. *Prog. Polym. Sci.* **2010**, *35*, 1350–1375. [[CrossRef](#)]
27. Gu, X.; Pang, Z.; Wei, Y.; Yang, R. On the influence of junction structures on the mechanical and thermal properties of carbon honeycombs. *Carbon* **2017**, *119*, 278–286. [[CrossRef](#)]
28. Wang, X.; Feng, Z.; Rong, J.; Zhang, Y.; Zhong, Y.; Feng, J.; Yu, X.; Zhan, Z. Planar net- $\tau$ : A new high-performance metallic carbon anode material for lithium-ion batteries. *Carbon* **2019**, *142*, 438–444. [[CrossRef](#)]
29. Peng, Q.; Meng, F.; Yang, Y.; Lu, C.; Deng, H.; Wang, L.; De, S.; Gao, F. Shockwave generates <100 > dislocation loops in bcc iron. *Nat. Commun.* **2018**, *9*, 4880. [[PubMed](#)]
30. Xie, L.; An, H.; Peng, Q.; Qin, Q.; Zhang, Y. Sensitive Five-Fold Local Symmetry to Kinetic Energy of Depositing Atoms in Cu-Zr Thin Film Growth. *Materials* **2018**, *11*, 2548. [[CrossRef](#)]
31. Plimpton, S. Fast Parallel Algorithms for Short-Range Molecular Dynamics. *J. Comput. Phys.* **1995**, *117*, 1–19. [[CrossRef](#)]
32. Juneja, A.; Rajasekaran, G. Anomalous strength characteristics of Stone-Thrower-Wales defects in graphene sheets - a molecular dynamics study. *Phys. Chem. Chem. Phys.* **2018**, *20*, 15203–15215. [[CrossRef](#)] [[PubMed](#)]
33. Dilrukshi, K.G.S.; Dewapriya, M.A.N.; Puswewala, U.G.A. Size dependency and potential field influence on deriving mechanical properties of carbon nanotubes using molecular dynamics. *Theor. Appl. Mech. Lett.* **2015**, *5*, 167–172. [[CrossRef](#)]
34. Xie, L.; An, H.; He, C.; Qin, Q.; Peng, Q. Mechanical Properties of Vacancy Tuned Carbon Honeycomb. *Nanomater. Basel* **2019**, *9*, 156. [[CrossRef](#)] [[PubMed](#)]
35. Stukowski, A. Visualization and analysis of atomistic simulation data with OVITO—the Open Visualization Tool. *Model. Simul. Mater. Sci. Eng.* **2010**, *18*, 015012. [[CrossRef](#)]
36. Hossain, M.Z.; Hao, T.; Silverman, B. Stillinger–Weber potential for elastic and fracture properties in graphene and carbon nanotubes. *J. Phys. Condens. Matter* **2018**, *30*, 055901. [[CrossRef](#)]
37. Vardimon, A.D.; Robbins, D.; Brosh, T. In-vivo von Mises strains during Invisalign treatment. *Am. J. Orthod. Dentofac. Orthop.* **2010**, *138*, 399–409. [[CrossRef](#)]
38. Rajasekaran, G.; Narayanan, P.; Parashar, A. Effect of Point and Line Defects on Mechanical and Thermal Properties of Graphene: A Review. *Crit. Rev. Solid State Mater. Sci.* **2015**, *41*, 47–71. [[CrossRef](#)]

